Journal of Ceramic Processing Research. Vol. 26, No. 4, pp. 661~671 (2025)
(Received 22 May 2025, Received in revised form 19 July 2025, Accepted 24 July 2025)
https://doi.org/10.36410/jcpr.2025.26.4.661

J O U R N A L O F
Ceramic Processing Research

Study on the distribution characteristics and solidification mechanism of heavy metal ions in polycrystalline slag glass-ceramics

Yuanjun Xu[a], Hongxia Zhang[a,*], Yongsheng Du[a], Zhishuang Pan[a] and Xuebing Xue[b]
[a]*College of Science, Inner Mongolia University of Science and Technology, Baotou 014010, China*
[b]*College of Materials Science and Engineering, Inner Mongolia University of Science and Technology, Baotou 014010, China*

This study established a resource utilization technology system for the blast furnace slag resource recovery (BFS). Using manganese-bearing blast furnace slag (MBFS) from Baotou Bayan Obo ore as the primary raw material, glass-ceramics were successfully prepared through the introduction of Cr_2O_3 and Fe_2O_3 composite nucleating agents. The research systematically elucidates the occurrence patterns and immobilization mechanisms of polymetallic elements (Cr, Mn, Pb) in glass-ceramics, providing theoretical support for high-value utilization of metallurgical solid waste. Experimental results demonstrated that the glass-ceramics exhibit a characteristic multi-phase composite structure: the augite phase as the primary crystalline phase grows attached to spinel, while the wollastonite phase interweaves with residual glass matrix. Heavy metal distribution analysis revealed that Cr and Mn were predominantly distributed within the spinel phase, whereas Pb showed enrichment in augite, wollastonite, and glass phases. Notably, elevated PbO content tends to induce localized lead-ion enrichment zones within the glass phase. The glass-ceramics achieved effective immobilization of multiple heavy metals through mechanisms such as "chemical fixation" and "physical encapsulation", as confirmed by heavy metal leaching tests and corrosion experiments.

Keywords: Manganese bearing blast furnace slag, Glass-ceramics, Heavy metals, Solidification mechanism.

Introduction

The rapid development of national economic construction has led to an increasing demand for mineral resources. It is noteworthy that in China's mineral resources, low-grade ores and refractory ores account for a high proportion with complex mineral compositions. Due to technological bottlenecks in mineral processing and economic constraints, the extraction, beneficiation, and smelting processes of these ores often lead to continuously increasing discharges of associated polymetallic tailings/slags [1-3]. For instance, the manganese-bearing blast furnace slag (MBFS) generated during the smelting of Baotou Bayan Obo iron ore represents a typical metallurgical solid waste. Over time, its accumulation has resulted in massive slag stockpiles [4]. The heavy metal elements present in BFS, such as Cr, Cu, Zn, and Mn, may diffuse into water bodies or soil and can accumulate in living organisms through bioaccumulation, posing a significant threat to the environment, as well as to human health via the food chain [5, 6].

At present, the comprehensive utilization of associated polymetallic tailings/slag resources includes the recovery of valuable metals, tailings/slag backfill, or the use of tailings/slag to prepare concrete, cement and other building materials [7-9]. Among them, glass-ceramics prepared from co-associated polymetallic tailings/slag exhibit high overall performance and are suitable for structural or decorative building applications [10-12]. For example, Li et al. successfully synthesized glass-ceramics via a one-step method using municipal solid waste incineration fly ash, chromium slag, lead-zinc tailings, and coal gangue as raw materials [13]. When the municipal solid waste incineration fly ash dosage reached 50%, the composite exhibited optimal comprehensive properties: a compressive strength of 226.85 MPa, a bulk density of 2.78 g/cm^3, and a water absorption rate of 0.64%. At this ratio, the sample demonstrated a dense internal microstructure with balanced crystal growth, achieving full compliance with Chinese construction material standards. Luo et al. used titanium-bearing BFS and granite tailings as the main raw materials [14], and successfully prepared slag glass-ceramics with a density of 3.02 g/cm^3 and a Vickers hardness of 8.6 GPa by the melting method, which can be used as decorative building materials.

Glass-ceramics produced from solid waste can also effectively solidify heavy metals. For example, Wang et al. prepared glass-ceramics using electrolytic manganese slag and ferrochromium slag as raw materials, and the successfully solidified heavy metals included Cr, Mn, Pb, Cd and Zn, etc [15]. Cr and Mn were mainly enriched in the spinel phase, while Pb, Cd, and Zn did not participate

*Corresponding author:
Tel : +86-472-5954358
Fax: +86-472-5954358
E-mail: zhanghongxia@imust.edu.cn

in the formation of crystalline phases but were uniformly dispersed in the glass matrix. The leaching concentrations of all heavy metals were far below the national standard limits, and the solidification rates all exceeded 99.9%. Li et al. prepared glass-ceramics using zinc leaching residue as the main raw material and studied the speciation and immobilization mechanisms of Pb, Zn, and Mn in the glass-ceramics [16]. The results indicate that Pb^{2+} replaces Ca^{2+} in anorthite and diopside crystals, while Zn^{2+} and Mn^{4+} replace Al^{3+} and Mg^{2+}/Fe^{2+}, respectively. These findings demonstrate that the immobilization efficiency of Pb ions varies across different glass-ceramics systems, depending on their specific incorporation mechanisms. Therefore, elucidating heavy metal solidification mechanisms in glass-ceramics is key to optimizing immobilization performance. Furthermore, as tailings/slag typically contain multiple heavy metal ions, their use as raw materials inevitably introduces diverse metallic elements into glass-ceramics. Understanding interactions among co-existing heavy metals in glass-ceramics matrices provides critical theoretical guidance for developing high-performance materials with low leaching rates using associated polymetallic tailings/slag.

In this study, MBFS was used as the main raw material to prepare SiO_2-CaO-MgO-Al_2O_3 (SCMA)-based slag glass-ceramics by the fusion method. By introducing a composite nucleating agent system of Cr_2O_3 and Fe_2O_3, nucleation and crystallization of the glass-ceramics were promoted. Additionally, the existential state of Pb, Cr, and Mn and their influence mechanisms on the nucleation and crystallization process were systematically investigated. The solidification efficiency of heavy metals within the glass-ceramics was quantitatively assessed via toxicity leaching tests and wheat seed germination experiments. By integrating microstructural analysis, the study further unveiled the underlying solidification mechanisms of heavy metals within the glass-ceramic matrix.

Experiment

Sample preparation

In this study, the MBFS originated from the Bayan Obo Mine, with its main chemical composition presented in Table 1. According to the SCMA system phase diagram, augite was identified as the main crystalline phase of the glass-ceramics. The base glass compositions comprised 47.43 SiO_2, 22.37 CaO, 8.81 MgO, and 7.39 Al_2O_3 (wt%) [17]. Thus, the formulation of glass-ceramics was determined (Table 2). To further promote nucleation and crystallization of the glass-ceramics, we achieved this by additionally adding nucleating agents Fe_2O_3 and Cr_2O_3. Based on previous research experience [18], when the addition ratio of Fe_2O_3 to Cr_2O_3 was 1:1, the glass-ceramics exhibited the optimal physicochemical properties. Since the amounts of SiO_2 and MgO provided by MBFS were insufficient to support the precipitation of augite, an additional appropriate amount of SiO_2 and MgO was required. Furthermore, Na_2CO_3 was added to lower the melting point of the glass during the melting process [18].

First, the raw materials were thoroughly mixed and placed in an alumina crucible, then melted at 1500 °C for 3 h to obtain a homogeneous glass melt. Next, a small amount of the glass melt was poured into ice water to obtain water-quenched samples for subsequent testing. The remaining glass melt was cast into a mold, placed in an annealing furnace at 600 °C, held for 5 h, and allowed to cool naturally to obtain annealed glass samples. The annealed sample was subjected to nucleation and crystallization treatment to obtain the final glass-ceramic samples.

Characterization techniques

The water-quenched glass samples were ground to pass through a 200-mesh sieve, and then loaded into an Al_2O_3 crucible to rise from room temperature to 1200 °C at standard atmospheric pressure for differential scanning calorimetry (DSC, NETZSCH 449) testing. Similarly, the powder of water-quenched glass samples were used for Raman spectroscopy (InVia) testing to analyze the effect of PbO on the glass network structure. The crystalline phase information of the glass-ceramics was obtained by testing with X-ray diffraction (XRD, Bruker D8 Advance). The sample used in this experiment was glass-ceramics powder (particle size less than 70 μm), and the scanning angle 2θ ranged from 10° to 80°.

Table 1. Chemical composition of MBFS (wt%).

Component	SiO_2	CaO	MgO	Al_2O_3	K_2O	Na_2O	TFe	TiO_2	MnO	REO
wt%	34.60	36.79	9.57	12.16	0.48	0.74	0.5	0.34	0.75	4.07

Note: TFe denotes Total Fe, and REO denotes the sum of rare earth oxides in the MBFS.

Table 2. Ingredients of MBFS glass-ceramics (wt%).

Sample	BFS	SiO_2	Na_2CO_3	MgO	Fe_2O_3	Cr_2O_3	PbO
Pb-1	63.2	27.4	3.7	3.1	1.3	1.3	1
Pb-2	63.2	27.4	3.7	3.1	1.3	1.3	2
Pb-3	63.2	27.4	3.7	3.1	1.3	1.3	3

The glass-ceramic samples were polished and observed for surface microstructure via field-emission scanning electron microscopy (FESEM, Gemini 300), combined with area scanning and point scanning analysis by energy-dispersive spectroscopy (EDS, Oxford, X-Max 50) to analyze element distribution. To further investigate the chemical state of Pb elements in the glass-ceramics, valence state analysis was performed using X-ray photoelectron spectroscopy (XPS, Thermo Kalpha) in this study. In accordance with the Toxicity Characteristic Leaching Procedure (TCLP) proposed by the U.S. Environmental Protection Agency, leaching experiments were designed to test the leaching concentration of heavy metals in glass-ceramics and evaluate the solidification effect. An acetic acid buffer system with pH=4.93±0.05 was selected as the leaching medium, which was mixed with glass-ceramic fragments with a particle size ≤9.5 mm at a liquid-solid ratio of 20:1 (L/kg) and oscillated for 20 hours. Finally, the leachate was detected by inductively coupled plasma mass spectrometry (ICP-MS, Agilent Technologies 5110) to obtain the leaching concentration results.

Results and Discussion

DSC analysis

In this study, the amorphous glass powder was prepared by the water quenching rapid cooling method, which ensured that the basic glass samples retained the structural characteristics of the original glassy state. Based on this, DSC tests were carried out, and the results are shown in Fig. 1. The characteristic temperature parameters of the curves include the glass transition temperature (T_g) and the crystallization exothermic peak temperature (T_p). It can be seen from the figure that there are two obvious crystallization exothermic peaks in the base glass. The more obvious crystallization exothermic peak (T_{p1}) may correspond to the main crystal phase of the glass-ceramics, while the weaker crystallization exothermic peak (T_{p2}) may correspond to the second phase of the glass-ceramics. According to relevant literature, the glass thermal stability parameter ΔT (ΔT = T_{p1}-T_g) is positively correlated with the degree of densification of the glass network structure [19]. Generally speaking, an increase in ΔT indicates that the glass network structure becomes more compact. According to the DSC curve of Fig. 1, ΔT is calculated, and the results are shown in Table 3. With the increase of PbO content, ΔT decreases gradually, indicating that the addition of PbO contributes to the depolymerization of glass network structure. Additionally, we can formulate the heat treatment regime for glass-ceramics based on the DSC curves. According to the relevant literature reports, the glass-ceramics are prepared by a two-step heat treatment method, and the appropriate nucleation temperature (around T_g~T_g+50 °C) and crystallization temperature (around T_p) are selected [20-22]. Therefore, the nucleation temperature of this experiment is 770 °C, and the crystallization temperature is 950 °C.

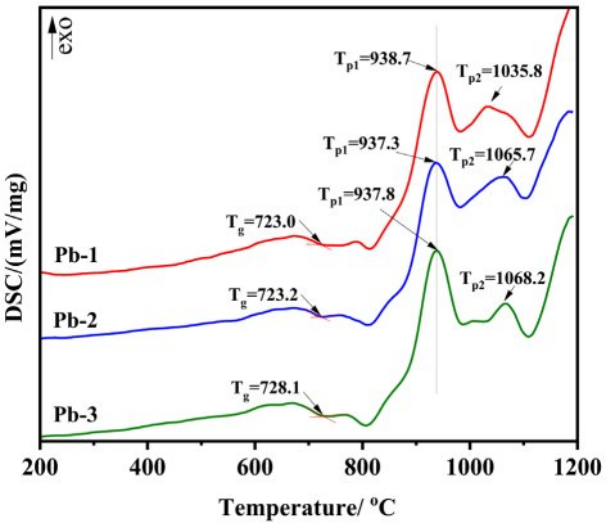

Fig. 1. DSC curves of the base glass samples with different PbO addition.

Table 3. Phase transition temperatures of the base glass samples.

Samples	Tg (°C)	Tp1 (°C)	ΔT (°C)
Pb-1	723.0	938.7	215.7
Pb-2	723.2	937.3	214.1
Pb-3	728.1	937.8	209.7

Raman spectra

To investigate the influence of PbO on the glass network structure, Raman spectra of base glasses with varying PbO contents were measured, as shown in Fig. 2(a). In the wavenumber range of 800-1200 cm^{-1}, the characteristic Raman bands are primarily attributed to the vibrational modes of bridging oxygen (BO) and non-bridging oxygen (NBO) in [SiO_4] tetrahedra [23, 24]. The structural units can be classified as Q^0 ([SiO_4]$^{4-}$, containing 4 NBOs), Q^1 ([Si_2O_7]$^{6-}$, containing 3 NBOs), Q^2 ([Si_2O_6]$^{4-}$, containing 2 NBOs), Q^3 ([Si_2O_5]$^{2-}$, containing 1 NBO), and Q^4 (SiO_2, containing no NBOs) [25]. The degree of network depolymerization can be evaluated by calculating the ratio of non-bridging oxygen to total oxygen (NBO/T) [26-28]. The Gaussian peak fitting of Raman spectra was performed by using Origin software. The Raman peaks of Q^0, Q^1, Q^2, and Q^3 were located in the range of 850-880, 900-920, 950-1000 and 1050-1100 cm^{-1}, respectively. The Q^4 Raman peak was not marked due to the low content. The relevant peak fitting results are shown in Fig. 2(b), (c) and (d). The formula for calculating NBO/T is given in Equation (1), and the results are listed in Table 4.

$$NBO/T = 0\times Q^4 + 1\times Q^3 + 2\times Q^2 + 3\times Q^1 + 4\times Q^0 \quad (1)$$

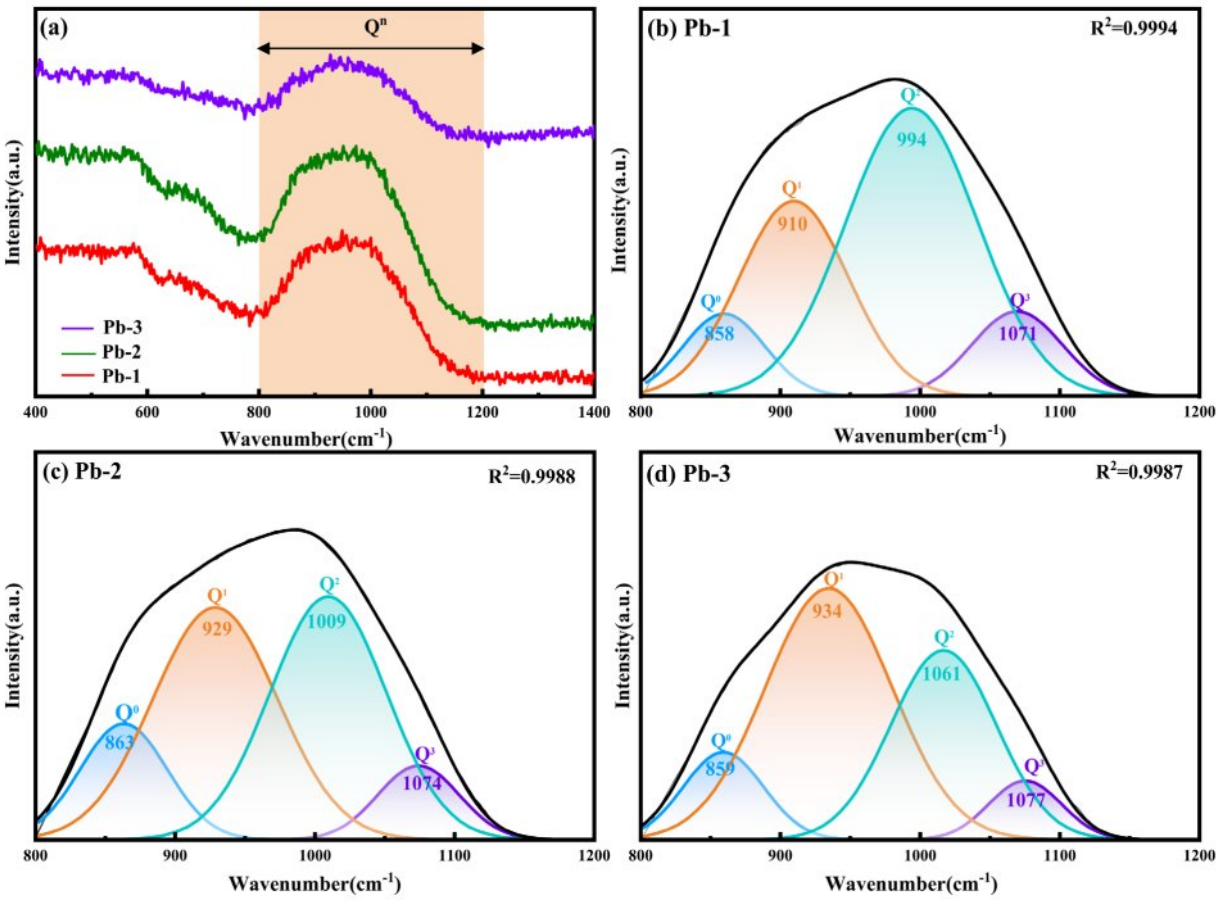

Fig. 2. (a) Raman spectra of base glass samples; (b) deconvoluted results of Pb-1; (c) deconvoluted results of Pb-2; (d) deconvoluted results of Pb-3.

Table 4. The value of Q^n and the calculation results of NBO/T of base glass samples with different PbO addition.

Sample	Q^0	Q^1	Q^2	Q^3	NBO/T
Pb1	8.99	29.04	51.47	10.5	2.37
Pb2	13.56	39.55	38.65	8.24	2.58
Pb3	10.91	50.57	31.73	6.79	2.66

As shown in Table 4, with the gradual increase in PbO content, the proportions of Q^0 and Q^1 exhibit an upward trend, whereas Q^2 and Q^3 show a downward trend. Consequently, the NBO/T ratio increases progressively, indicating a gradual rise in the depolymerization degree of the glass network structure. This demonstrates that the introduction of PbO disrupts the [Si-O] network, reducing its structural integrity. Such network depolymerization helps lower the viscosity of the glass system, thereby facilitating subsequent crystallization processes [29]. These conclusions align with the results obtained from DSC analysis.

Phase analysis

Fig. 3 reveals the crystalline phase evolution rules in glass-ceramics with different PbO doping amounts through XRD technology. By comparing with standard PDF cards, it can be seen that all samples exhibit a multiphase structural feature with augite ((Ca,Na)(Mg,Fe,Al,Ti)$(Si,Al)_2O_6$) as the main crystalline phase and wollastonite ($CaSiO_3$) as the secondary crystalline phase. Spinel formed by the composite nucleating agents Fe_2O_3 and Cr_2O_3 acts as nuclei to promote the formation of the main crystalline phase augite [18]. The formation of wollastonite is due to the fact that the MBFS is rich in Ca elements, and the Ca elements provides a component

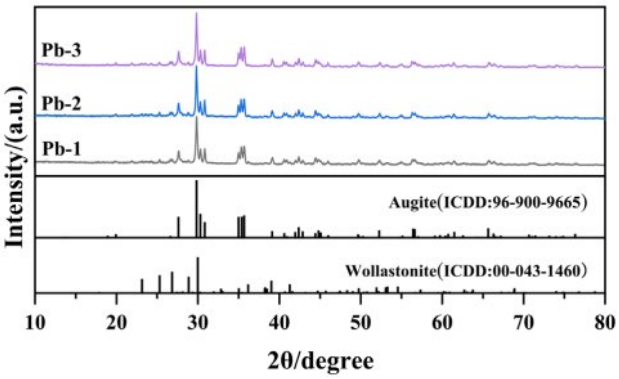

Fig. 3. XRD patterns of glass-ceramics with different PbO contents.

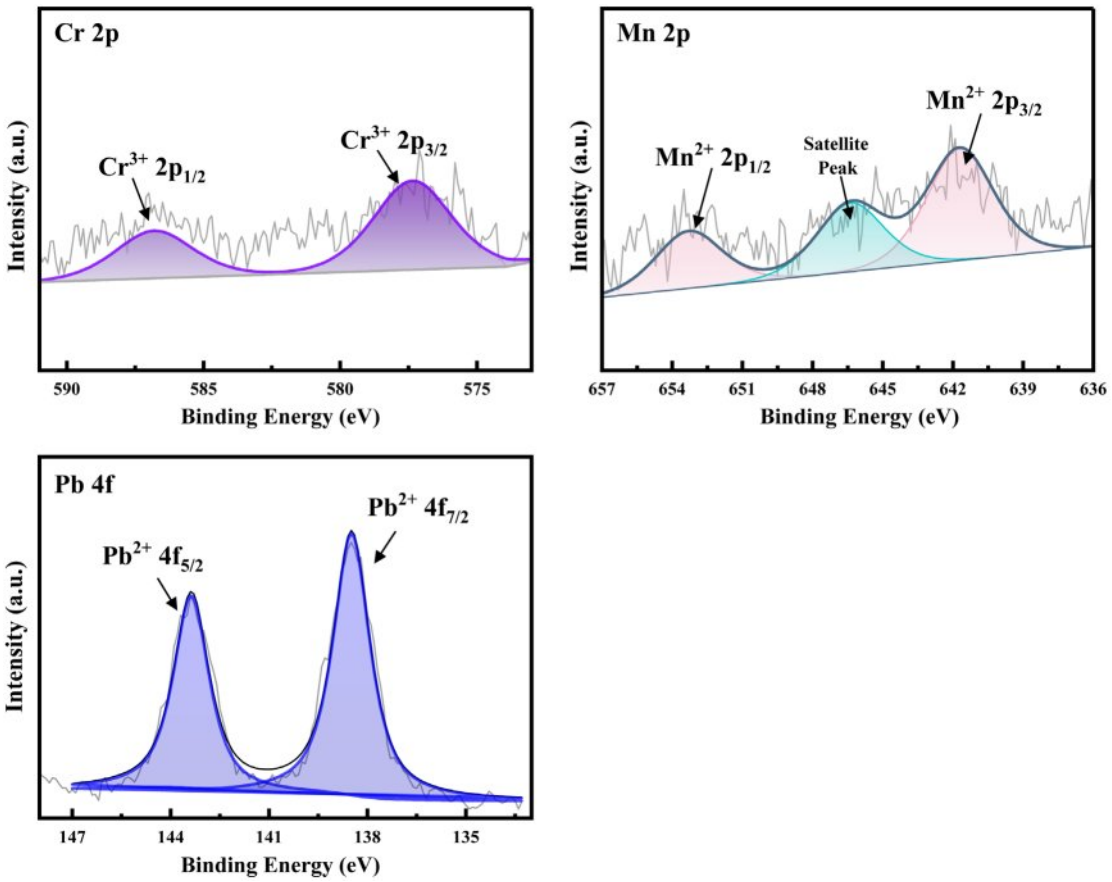

Fig. 4. XPS fitting spectra of heavy metals Cr, Mn, and Pb in sample Pb-3.

basis for the formation of wollastonite [30]. At the same time, it is found that the increase of PbO content had no significant effect on the crystal type of glass-ceramics, indicating that the addition of PbO cannot lead to the formation of Pb-containing second phase in glass-ceramics.

Valence state analysis of Pb ion

In order to determine the valence states of heavy metals such as Cr, Mn, and Pb in the prepared glass-ceramics, XPS detection was performed on the glass-ceramics sample Pb-3, and the relevant results are shown in Fig. 4. Through the curve fitting of the XPS spectra, it was analyzed and confirmed that Cr is in the +3 valence state, and the chemical valence states of Mn and Pb are +2. This result is consistent with existing research reports and also indicates that there is no transition of chemical valence states before and after heat treatment [31-33].

Micro-morphology and elemental composition analysis

To investigate the phase distribution characteristics and heavy metal distribution of glass-ceramics with different PbO contents, FESEM combined with EDS surface scanning was used to characterize the microstructure and element distribution of polished samples (Fig. 5). Combined with XRD phase analysis, it was found that: the enrichment of Cr element in region a corresponds to the spinel phase, which acts as a heterogeneous nucleation site to effectively promote the formation of the main crystalline augite phase (Mg enrichment in region c); the enrichment of Al element in region b represents the glassy phase matrix; and the enrichment of Ca element in region d matches the characteristics of the wollastonite phase. This is due to the fact that Fe_2O_3 and Cr_2O_3 can first form the chromium-containing spinel crystal nucleus during the nucleation and crystallization heat treatment of the glass-ceramics. The spinel crystal nucleus interface can be a substrate for heterogeneous nucleation and promote the main crystal phase to precipitate in a dendritic form. Wollastonite is located at the edge of augite. Further analysis shows that in addition to the enrichment of heavy metal Cr element, Mn element is also enriched in spinel, indicating that spinel crystal can effectively solidify these heavy metal elements. The EDS surface scanning results also show that with the gradual increase of PbO content, the Pb-rich white region e gradually appears in the glass-ceramics. The absence of discrete Pb-bearing crystalline phases in XRD patterns, despite increasing PbO content, combined with the spatial coincidence of Pb and Al enrichment zones in elemental mapping, conclusively identifies these regions as Pb-incorporated glassy phases [34].

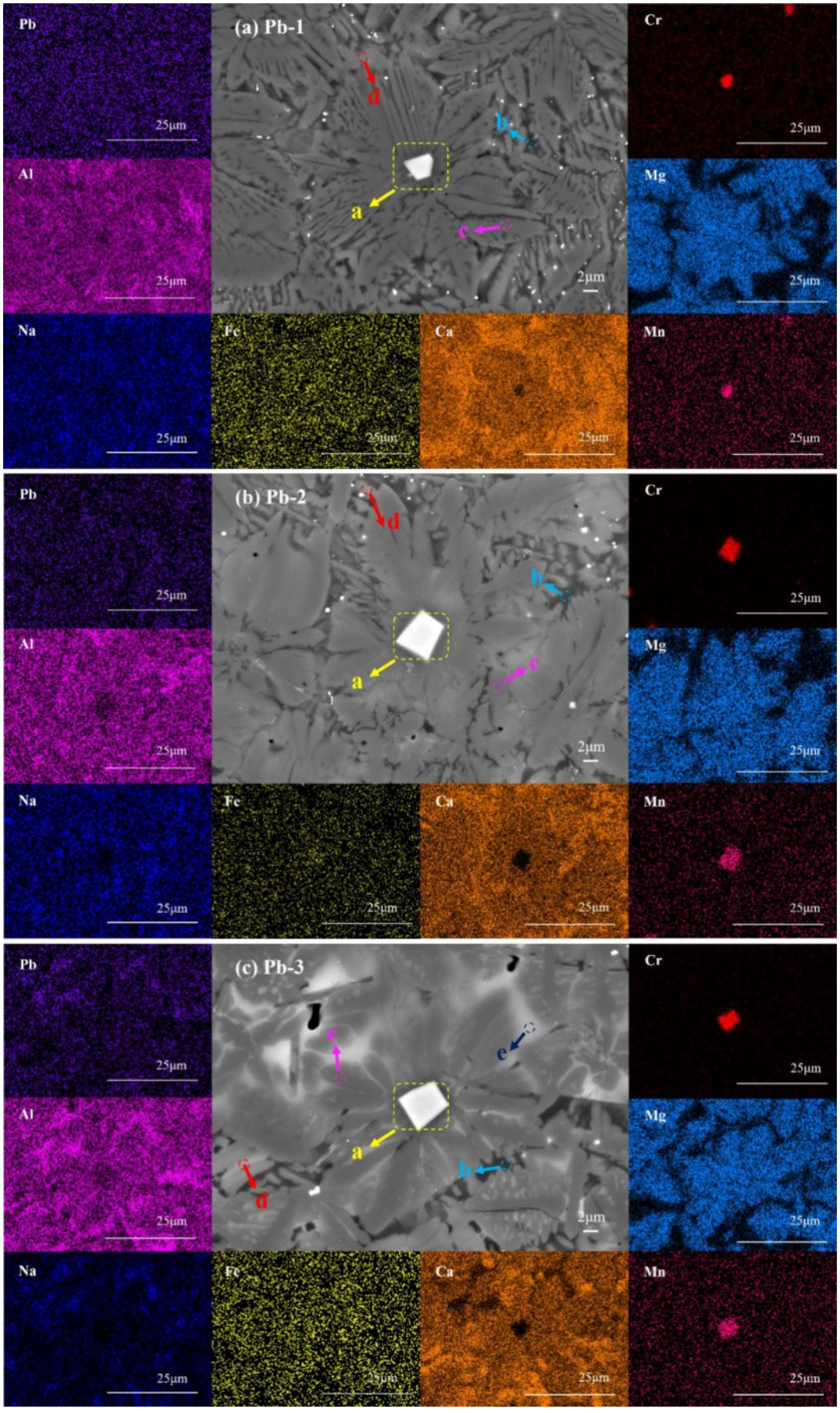

Fig. 5. FESEM and EDS element mapping of glass-ceramics with different PbO addition: (a) Pb-1; (b) Pb-2; (c) Pb-3.

To systematically evaluate the PbO-dependent elemental distribution in glass-ceramics, EDS point scanning analysis was performed on polished samples (Fig. 6). The spinel phase (region a) main elements includes Cr, Mg, Al, Fe, Mn and O (molecular formula: $(Mg,Fe,Mn)(Al,Cr,Fe)_2O_4$), demonstrating effective stabilization of Cr and Mn heavy metals. The augite phase (region c) incorporated multiple cations including Pb^{2+}, with its chemical composition represented as $(Ca,Mg,Na,Fe,Mn,Pb)(Mg,Fe,Al)(Si,Al)_2O_6$. As the PbO content increases progressively, the concentration of Pb^{2+} in augite rises correspondingly, while the content of Ca^{2+} decreases proportionally. This phenomenon confirms that Pb^{2+} can substitute for Ca^{2+} to incorporate into the augite structure. The underlying mechanism lies in the close similarity of ionic radii between Pb^{2+} (1.19 Å) and Ca^{2+} (1.00 Å), which facilitates the isomorphic substitution of these ions within the augite lattice [16, 35]. The main elements of the wollastonite phase include Ca, Pb, Mg, Al, Na, Si, O, etc., and the corresponding molecular formula is $(Ca,Pb,Mg,Na)(Si,Al)O_3$. Pb^{2+} incorporation through isovalent substitution for Ca^{2+}

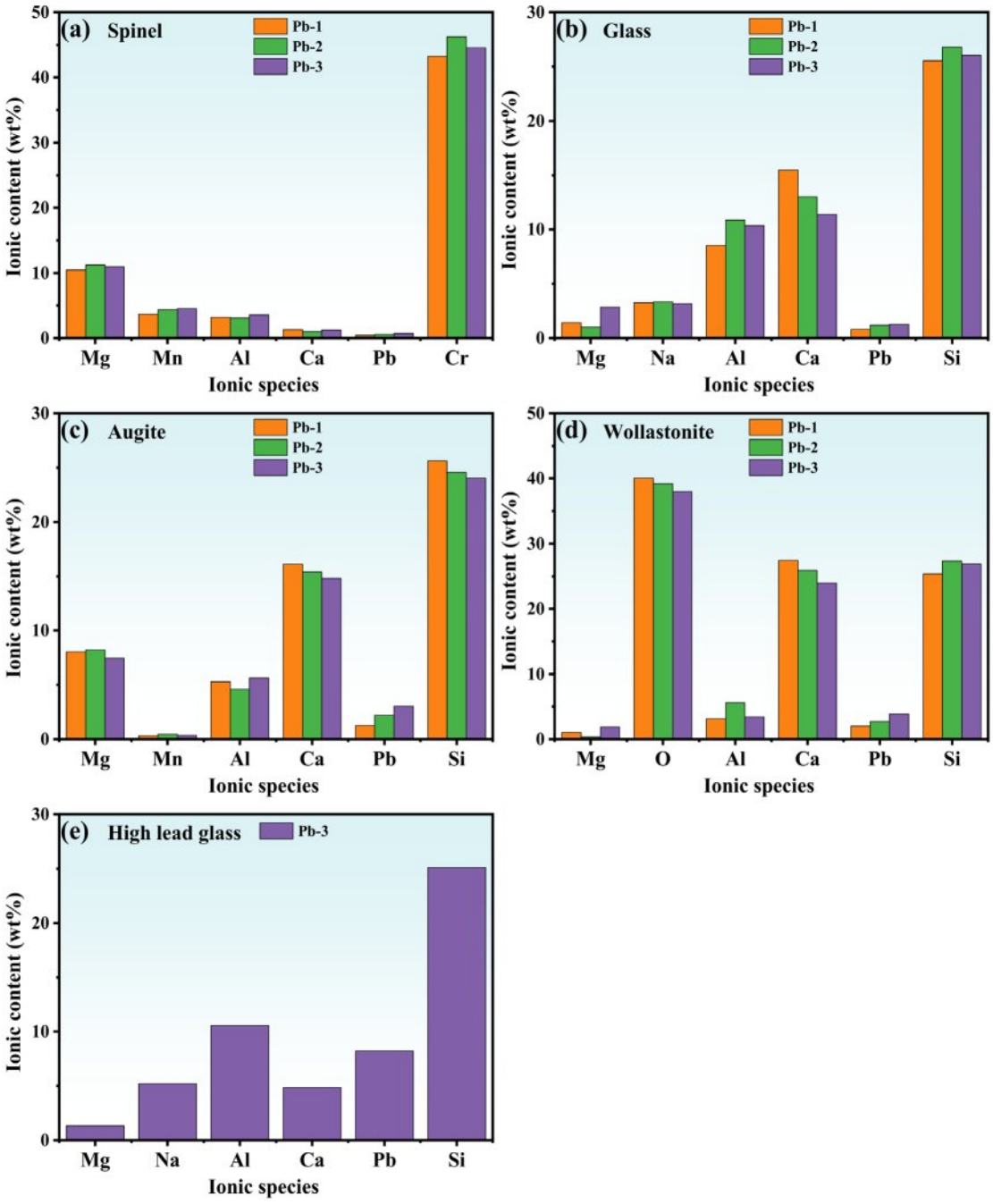

Fig. 6. EDS point scans of glass-ceramics with different PbO addition: (a) spinel; (b) glass; (c) augite; (d) wollastonite; (e) high lead glass.

occurs in the wollastonite crystal lattice, facilitated by their comparable ionic radii. The elements in the glass phase mainly include Si, Al, O, Na, Ca, Pb, etc. $[SiO_4]$ and $[AlO_4]^-$ are the base structural units that constitute the glass network, and Na^+ plays the role of equilibrium valence in the $[AlO_4]^-$ tetrahedron. The Ca^{2+} ions in the glass phase will destroy the [Si-O] and [Al-O] network structure, reduce the integrity of the glass network structure, and thus facilitate the crystallization of the glass-ceramics. With the gradual increase of PbO content, there is also ion substitution between Ca^{2+} and Pb^{2+} in the glass phase. In particular, when the content of PbO in the glass-ceramics is large, the lead ion enrichment region is easily formed in some glass phases, and the corresponding lead ion content is up to 8.23 wt%. Similarly, the enrichment of Cr^{3+} and Mn^{2+} in the spinel phase is attributed to Cr^{3+} (0.63 Å) substituting for Al^{3+} (0.54 Å) at the octahedral sites of the spinel [36]. For Mn^{2+}, its ionic radius (0.83 Å) is comparable to that of other cations in the spinel (such as Mg^{2+} (0.72 Å) and Fe^{2+} (0.76 Å)), which creates favorable conditions for Mn^{2+} to enter the spinel lattice [12].Combined with the above analysis, the glass-ceramics can solidify the heavy metal Cr, Mn and Pb elements in the crystal through the spinel phase, augite phase and wollastonite, and the glass phase can also solidify most of the heavy metal Pb elements by physical coating solidification [37], thus realizing the effective solidification of a variety of heavy metals.

Table 5. Leaching test results of glass-ceramics with different PbO addition (mg/L).

Element	TCLP standard limits	Pb-1	Pb-2	Pb-3
Pb	5	0.067	0.086	0.102
Cr	5	0.044	0.037	0.041
Mn	5	0.047	0.055	0.044

Heavy metal leaching characteristics

This study employed the TCLP standard to quantita-

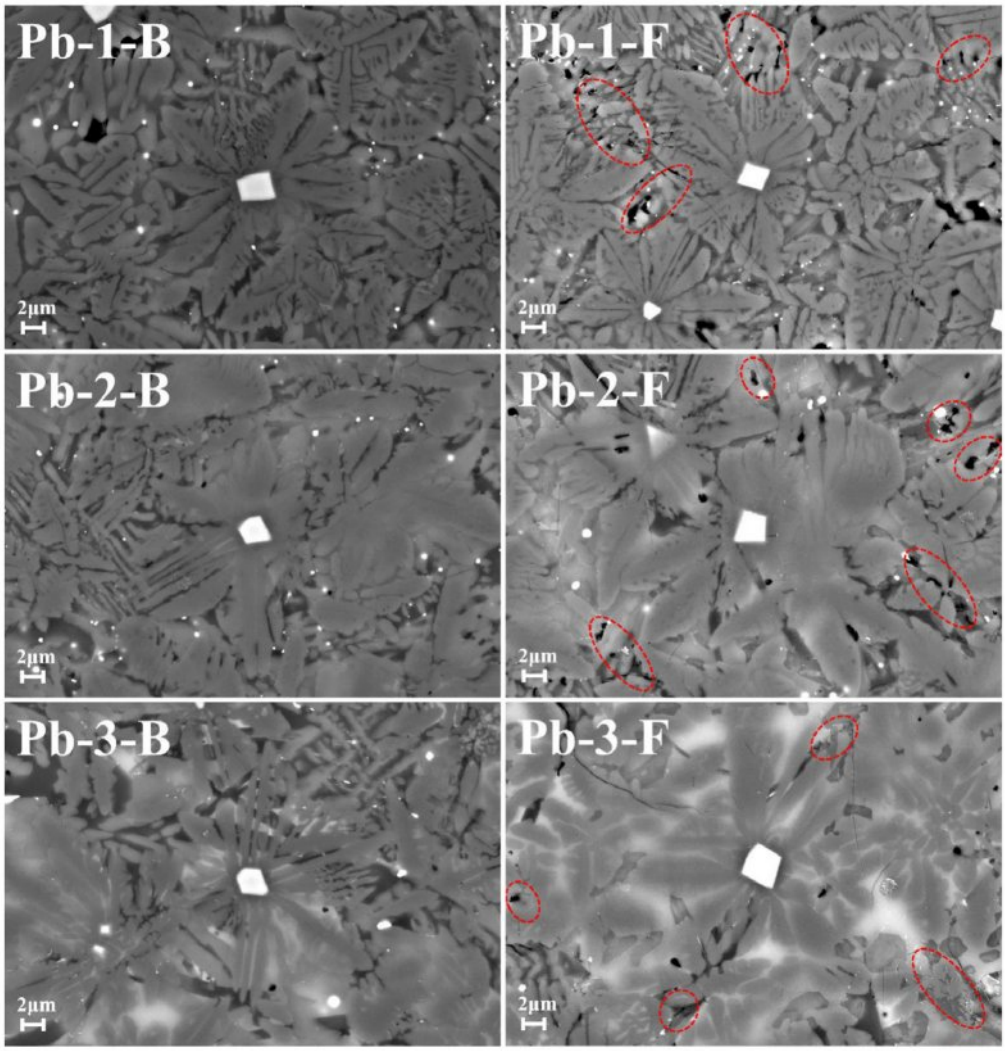

Fig. 7. Comparison of surface morphology before and after leaching corrosion in glass-ceramics with different PbO addition.

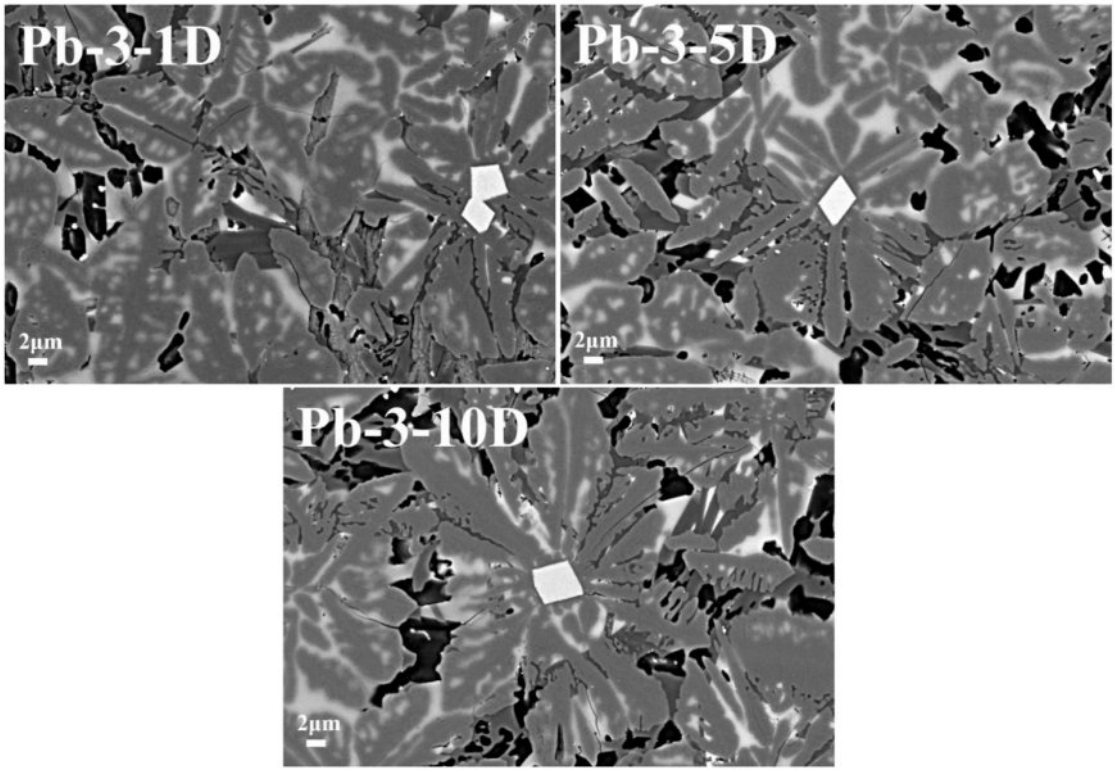

Fig. 8. Surface morphology of glass-ceramics sample Pb-3 with different corrosion time.

tively characterize the heavy metal immobilization performance of glass-ceramics. As shown in Table 5, the toxic leaching test results demonstrate that the leaching concentrations of Cr, Mn, and Pb ions are significantly lower than the standard limits. Notably, the leaching concentration of Pb ions exhibits an increasing trend with higher PbO doping levels. This phenomenon may be attributed to the superior corrosion resistance of the crystalline phase compared to the glass phase during the corrosion process of glass-ceramic [38]. Fig. 7 shows the surface morphology of glass-ceramics with different PbO content after being corroded by acetic acid solution in TCLP standard for 20 h. The comparison shows that there are obvious corrosion pits between the grain boundary of the glass-ceramics after corrosion, as shown in the red circle in Fig. 7 This may be due to the corrosion of the glass phase between the grain boundaries. Because most of the Pb ions in the glass-ceramics are distributed in the glass phase, the leaching value increases with the increase of the added PbO content [39].

In order to further study the change rule of the surface morphology of glass-ceramics under the corrosion of acetic acid solution in TCLP standard, the surface morphology of Pb-3 glass-ceramics samples with corrosion time of 1, 5 and 10 days is compared and analyzed. The results are shown in Fig. 8. It can be seen that the corrosion of glass-ceramics first occurs at the grain boundary and defects. Under the action of acid solution, the grain boundary will become the diffusion channel of H^+ ions and continue to expand [40]. Then the glass phase will be gradually peeled off from the grain boundary, and the glass network structure will be gradually destroyed, so that it will eventually form isolated silicate units and then be dissolved by acid solution. As the corrosion time continues to increase, the grain boundary of the augite phase gradually becomes clear and its width gradually increases, and some augite dendrites begin to be corroded. This may be due to the substitution of metal ions in augite by H^+, which makes the crystal structure unstable and therefore corroded by acid solution [41]. In addition, it is also found that there are small corrosion cracks on the surface of the sample as the corrosion proceeds. This may be due to the ion exchange under the acid solution, the H^+ with smaller ion radius replaces the metal ions in the silicate network structure unit, resulting in tensile stress on the surface of the sample, which will crack when the tensile stress reaches the limit.

Seed germination experiment

To evaluate the ecological safety of glass-ceramics, this study conducted biological toxicity testing using a wheat seed germination experiment. Glass-ceramics raw material powder and crystallized sample powder are separately immersed in deionized water at a solid-to-liquid ratio of 1:10 (g/mL) for 5 days to collect the resulting leachates. Meanwhile, deionized water served as the blank control. Ten uniformly sized wheat seeds from

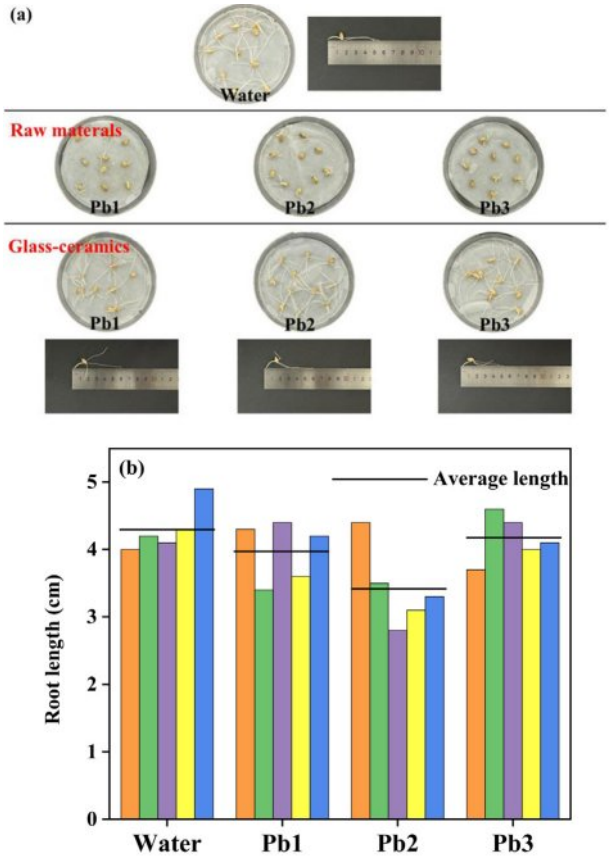

Fig. 9. (a) All control group seed rooting and germination photos. (b) Root growth length of wheat seeds.

each group underwent dark cultivation in the respective leachates. After 3 days, germination morphology are obtained in Fig. 9(a) and it revealed that seeds soaked in raw material leachate exhibited significantly restricted radicle development, indicating notable biotoxicity of untreated materials. In contrast, the germination rate and primary root elongation in glass-ceramics powder leachate show no statistical differences from the control group, confirming crystallized sample's toxicity with negligible environmental and biological impacts. Quantitative analysis of radicle growth parameters are shown in Fig. 9(b). The result demonstrated that the average root length in glass-ceramics leachate was slightly reduced compared to controls, a difference attributed to Pb^{2+} leaching from glass-ceramics. Pb^{2+} can inhibit cytokinin synthesis in plant cells, thereby affecting root development. Comprehensive results demonstrate that the glass-ceramics material prepared in this study exhibits excellent ecological safety after high-temperature reconstruction.

Conclusion

In this study, MBFS, a type of metallurgical solid waste, was used as the main raw material. Combined with a Cr_2O_3 and Fe_2O_3 composite nucleating agent system, environmentally friendly glass-ceramics were prepared via a high-temperature melting-controlled crystallization process. By adding an appropriate amount of PbO, the study systematically revealed the dual stabilization mechanisms of heavy metal elements such as Pb, Cr, and Mn in the glass-crystal composite system. Through multi-scale verification of experimental results using various characterization techniques, the following conclusions were drawn:

1. The glass-ceramics prepared with Cr_2O_3 and Fe_2O_3 as composite nucleating agents have excellent crystallization characteristics. Cr_2O_3 contributes to the formation of chromium-containing iron spinel nuclei in the glass-ceramics, while augite phase is attached to the epitaxial growth of spinel nuclei in the form of dendrites.

2. Phase analysis shows that the glass-ceramic system exhibits a multiphase composite structure of spinel phase, augite phase, wollastonite phase and glass phase. Doping of PbO does not alter the type of main crystalline phases. However, Raman spectroscopy analysis indicates that the network-breaking effect of Pb^{2+} leads to the depolymerization of the glass network, thereby enhancing the crystallization characteristics of the glass-ceramics.

3. The heavy metal ions such as Pb, Cr and Mn in glass-ceramics can be chemically fixed by entering the spinel phase, augite phase and wollastonite phase lattice. At the same time, the glass phase can also solidify Pb ions by physical encapsulation, indicating that the MBFS glass-ceramics have excellent solidification ability for a variety of heavy metals. The results of the TCLP show that the leaching concentrations of Pb, Cr, and Mn are as low as 0.067 mg/L, 0.037 mg/L, and 0.044 mg/L, respectively, which are two orders of magnitude lower than the standard limits. In the concurrent wheat seed germination experiment, there was no significant difference in rooting and germination between wheat seeds cultivated with the glass-ceramics leachate and the blank control group (deionized water), indicating that the glass-ceramics exhibit excellent solidification efficiency and high ecological safety.

Acknowledgments

This work was supported by the Natural Science Foundation of the Inner Mongolia Autonomous Region (grant number 2023MS05035), Fundamental Research Funds for the Inner Mongolia University of Science & Technology (2023QNJS121).

References

1. L. Liu, H. Yu, Y.L. Li, and Z.K. Zhang, J. Clean. Prod. 269 (2020) 122417.
2. G.H. Ai, Y.F. Liu, Y. Wang, and Y.L. Chen, J. Residuals Sci. Technol. 12 (2015) 17-23.
3. E. Stoltz and M. Greger, Plant Soil 289 (2006) 199-210.
4. W.B. Li, J.J. Chen, W.T. Zhou, Y.X. Han, and Y. Shan, Int. J. Min. Sci. Technol. 32 (2022).

5. J.J. Zhang, B. Liu, and S.G. Zhang, Sci. Total Environ. 781 (2021) 146727.
6. Z.Y. Bai, F.Z. Wu, Y.P. He, and Z.W. Han, Environ. Pollut. Bioavail. 35 (2023) 2156397.
7. Y.L. Zhao, J.P. Qiu, Z.Y. Ma, Z.B. Guo, and H. Lui, Powder Technol. 375 (2020) 539-548.
8. H. Park, Y. Jeong, Y.B. Jun, and J.E. Oh, Constr. Build. Mater. 122 (2016) 343-353.
9. C. Li, Q.J. Wen, M.Z. Hong, Z.Y. Liang, Z.Y. Zhuang, and Y. Yu, Constr. Build. Mater. 134 (2017) 443-451.
10. Y. Niu, F. Zheng, Y. Liu, Y. Yang, T. Yu, Z. Wang, X. Mao, Q. Zhen, and Y. Yu, Ceram. Int. 50 (2024) 39983-39992.
11. L. Zhang, L. Liang, Y. Li, J. Chen, Z. Cui, J. Qiao, Z. Zhang, Z. Wang, Q. Xu, and C. Zhao, Ceram. Int. 50 (2024) 43699-43709.
12. G.Y. Wang, Y.S. Du, Y.H. Guo, H.X. Zhang, L.B. Deng, H. Chen, and M. Zhao, Environ. Prog. Sustain. Energy 42 (2023) e14019.
13. C.W. Li, P.P. Zhang, L.H. Zeng, L. Yu, and D.W. Li, J. Build. Eng. 68 (2023) 106080.
14. Y.L. Luo, F. Wang, H.Z. Zhu, Q.L. Liao, Y.L. Xu, and L.B. Liu, J. Non-Cryst. Solids 582 (2022) 121463.
15. J.Q. Wang, F.L. Han, B.G. Yang, Z.B. Xing, and T.T. Liu, Front. Chem. 10 (2022) 989087.
16. C.B. Li, G.F. Zhang, H. Zheng, F. Zhang, and K. Liu, J. Clean. Prod. 426 (2023) 139021.
17. W.X. Shang, Z.W. Peng, Y.W. Huang, F.Q. Gu, J. Zhang, H.M. Tang, L. Yang, W.G. Tian, M.J. Rao, G.H. Li, and T. Jiang, J. Clean. Prod. 317 (2021) 128220.
18. G.Y. Wang, Y.S. Du, J. Ma, H.X. Zhang, S.L. Ouyang, L.B. Deng, H. Chen, and M. Zhao, J. Ceram. Process. Res. 22[6] (2021) 665-674.
19. Y.S. Du, Y.H. Guo, G.Y. Wang, H.X. Zhang, L.B. Deng, H. Chen, and M. Zhao, J. Mater. Cycles Waste 25 (2023) 3081-3092.
20. Z.B. Pan, Q.K. Wang, H.Q. Wang, L.S. Yang, X.H. Zhu, S.N. Lin, Y.Y. Lv, J. Zheng, W.J. Duan, and J.L. Liu, J. Non-Cryst. Solids 646 (2024) 123263.
21. J.H. Huang, J.H. Zhang, Y.J. Yu, H.T. Bai, Z.L. Zhang, and Y.Q. Huang, J. Non-Cryst. Solids 588 (2022) 121585.
22. H.L. Shen, B. Liu, Y. Liu, J.J. Zhang, J. Liu, and S.G. Zhang, J. Alloys Compd. 911 (2022) 165010.
23. Y.X. Zhang, S.L. Liu, S.L. OuYang, X.F. Zhang, Z.W. Zhao, X.L. Jia, Y.S. Du, L.B. Deng, and B.W. Li, Mater. Chem. Phys. 252 (2020) 123061.
24. M. Liu, L.J. Zhao, Y. Liu, Z.J. Lan, L.F. Chang, Y.M. Li, and H. Yu, J. Mater. Sci. Technol. 30 (2014) 1213-1216.
25. J.F. Yu, Z.W. Peng, W.X. Shang, Q.X. Chen, G.Y. Zhu, H.M. Tang, M.J. Rao, and G.H. Li, Ceram. Int. 49 (2023) 15947-15958.
26. X.H. Geng, Z.W. Zhu, J.W. Cao, Z. Wang, J.S. Lu, and G.Y. Qian, Ceram. Int. 47 (2021) 13874-13883.
27. L.B. Deng, B. Yao, W.W. Lu, M.X. Zhang, H. Li, H. Chen, M. Zhao, Y.S. Du, M.R. Zhang, Y.H. Ma, and W.C. Wang, J. Non-Cryst. Solids 593 (2022) 121770.
28. J. Cheng, Z. Xiao, K. Yang, and H. Wu, Ceram. Int. 39 (2013) 4055-4062.
29. Y.S. Du, Y. Wei, Z.C. Zheng, Y.H. Guo, H.X. Zhang, L.B. Deng, H. Chen, and M. Zhao, J. Ceram. Process. Res. 25[2] (2024) 268-277.
30. Y. Wei, Y.S. Du, Y.H. Guo, D.Y. Zhao, H.X. Zhang, L.B. Deng, H. Chen, and M. Zhao, Ceram. Int. 50 (2024) 39516-39527.
31. W.T. Zou, W.H. Zhang, Y.L. Pi, Y.S. Zhang, L. Zhang, and Y. Chen, Ceram. Int. 48 (2022) 5040-5053.
32. L. Liu, H. Yu, Y.L. Li, and Z.K. Zhang, J. Clean. Prod. 269 (2020) 122417.
33. W.T. Zou, W.H. Zhang, Y.L. Pi, Y.S. Zhang, Y. Chen, and L. Zhang, Ceram. Int. 48 (2022) 36166-36177.
34. F.K. Wang, B.Q. Xu, B. Yang, and T.T. Shi, J. Hazard. Mater. 429 (2022) 128334.
35. W.F. Song, Z.W. Zhu, J.W. Cao, Z. Wang, J.S. Lu, and G.Y. Qian, J. Non-Cryst. Solids 563 (2021) 120809.
36. Y. Hao, S. Wang, and Y.B. Zhang, J. Lumin. 242 (2022) 118542.
37. S.Z. Zhao, Q. Wen, X.Y. Zhang, B. Liu, and S.G. Zhang, Ceram. Int. 47 (2021) 21599-21609.
38. D.Y. Zhao, Y.S. Du, Y.H. Guo, Y. Wei, H.X. Zhang, L.B. Deng, H. Chen, and M. Zhao, J. Alloys Compd. 1030 (2025) 180902.
39. S.Z. Zhao, B. Liu, Y.J. Ding, J.J. Zhang, Q. Wen, C. Ekberg, and S.G. Zhang, J. Clean. Prod. 271 (2020) 122674.
40. P.P. Zhang, L.H. Zeng, S.H. Zhang, C.W. Li, and D.W. Li, Environ. Sci. Pollut. R. 30 (2023) 29392-29406.
41. H.X. Zhang, Y.S. Du, X.W. Yang, X.F. Zhang, M. Zhao, H. Chen, S.L. Ouyang, and B.W.,Li, J. Non-Cryst. Solids 482 (2018) 105-115.